

Light scattering from cells: finite-difference time-domain simulations and goniometric measurements

Rebekah Drezek, Andrew Dunn, and Rebekah Richards-Kortum

We have examined the light-scattering properties of inhomogeneous biological cells through a combination of theoretical simulations and goniometric measurements. A finite-difference time-domain (FDTD) technique was used to compute intensity as a function of scattering angle for cells containing multiple organelles and spatially varying index of refraction profiles. An automated goniometer was constructed to measure the scattering properties of dilute cell suspensions. Measurements compared favorably with FDTD predictions. FDTD and experimental results indicate that scattering properties are strongly influenced by cellular biochemical and morphological structure. © 1999 Optical Society of America

OCIS codes: 170.3660, 290.0290.

1. Introduction

A. Background

Increasing the present understanding of the interaction of light with tissue at a cellular level will promote the development of optical diagnostic techniques potentially capable of rapid, noninvasive assessment of tissue pathology. In the past few years, a number of techniques have been developed that rely in some manner on measuring the scattering properties of tissue to determine physiological state. These techniques range from direct imaging methods such as confocal microscopy¹ and optical coherence tomography,² to more indirect approaches including elastic-scattering spectroscopy³ and photon migration.⁴

It is known that light scattering from tissue is dependent on the tissue's morphological and biochemical structure. However, the details of this dependence are not fully understood. As a result, although many elastic-scattering methods are able to measure differences between normal and diseased tissue, it is difficult to meaningfully relate measurements to specific underlying chemical and physical changes. Furthermore, without a sufficient quantitative model capable

of predicting elastic scattering based on changes in tissue on a microscopic level, it is challenging to make *a priori* predictions of how effectively a particular optical diagnostic technique will be able to detect disease in a specific tissue. In addition, lack of accurate, quantitative models makes it difficult to assess how variations in optical system design might be able to enhance differences between normal and diseased tissue, improving the diagnostic performance of the instrument.

Until recently, exploring the relationship between cell structure and light scattering was difficult because there was not a mathematical model for predicting scattering for complex biological cells. Because of the size of scatterers in cells relative to the wavelengths used in optical imaging, electromagnetic methods are required to describe scattering. Mie theory has been used extensively to approximate scattering but generally requires modeling a cell as a homogeneous sphere. Schmitt and Kumar have presented a useful expansion of this idea by applying Mie theory to a volume of spheres with various sizes distributions.⁵ Another approach more general than Mie theory involves calculating the light scattered from a coated sphere. In the coated sphere model, the sphere and the coating each have a distinct index of refraction, which makes it possible to model a spherical cell containing a homogeneous spherical nucleus.⁶ More recently, anomalous diffraction approximations,⁷ multipole solutions,⁸ and *T*-matrix computations⁹ have been proposed and implemented. Each of these techniques offers significant advantages over conventional Mie theory; however, all require limiting geometric and refractive-index assumptions.

R. Drezek and R. Richards-Kortum are with the Biomedical Engineering Program, University of Texas at Austin, Engineering Science Building, Room 610, Austin, Texas 78712. A. Dunn is with the Beckman Laser Institute and Medical Clinic, University of California, Irvine, Irvine, California 92697-1875.

Received 2 October 1998; revised manuscript received 16 February 1999.

0003-6935/99/163651-11\$15.00/0
© 1999 Optical Society of America

A more flexible approach is provided by a three-dimensional finite-difference time-domain (FDTD) model of cellular scattering.¹⁰ Although computationally intensive, this model allows the computation of scattering patterns from inhomogeneous cells of arbitrary shape. The aim of the research described in this paper is to develop an increased understanding of how light interacts with tissue on a cellular level using the FDTD model to predict cellular scattering patterns. The research reported in this paper expands upon our previous research in the field. We implement cell dielectric structure in a more realistic manner, for example, by incorporating fluctuations in refractive index within the nucleus rather than modeling the nucleus as a homogeneous structure. We investigate how scattering is influenced by changes in nuclear size and refractive index, by changes in organelle size, refractive index, and volume fraction, and by changes in the refractive index of the medium surrounding a cell. We simulate scattering from a collagen fiber. We investigate the wavelength dependence of scattering patterns and scattering cross section. Finally, to provide a comparison for theoretical FDTD predictions, an automated goniometer is used to experimentally measure the phase functions and asymmetry parameters of cell suspensions.

B. Cell Structure

Because scattering arises from mismatches in refractive index, when considering a cell from the perspective of how it will interact with light, the cell is viewed more appropriately as a continuum of refractive-index fluctuations than as a single object containing a number of discrete particles. The magnitude and spatial extent of the index of refraction fluctuations arise from the physical composition and size of the components that make up the cell. Organelles and subcomponents of organelles having indices different from their surroundings are expected to be the primary sources of cellular scattering. The cell itself may be a significant source of small-angle scatter in applications such as flow cytometry in which cells are measured individually; however, for *in vivo* scattering-based diagnostics, the cell as an entity is not as important because cells will be surrounded by other cells or tissue structures of similar index.

Certain organelles in cells are important potential sources of scattering. The nucleus is significant because it is often the largest organelle in the cell and its size increases relative to the rest of the cell throughout neoplastic progression. Other potential scatterers include organelles whose size relative to the wavelength of light suggests that they may be important backscatterers. These include mitochondria (0.5–1.5 μm), lysosomes (0.5 μm), and peroxisomes (0.5 μm). Mitochondria may be particularly influential in those cells that contain significant mitochondrial volume fractions because of this organelle's unique folded membrane structure. For example, Beauvoit *et al.* have found that mitochondria contribute 73% of the scattering from hepatocytes.¹¹ In addition, melanin, traditionally thought

of as an absorber, must be considered an important scatterer because of its size and high refractive index. Finally, structures consisting of membrane layers such as the endoplasmic reticulum or Golgi apparatus may prove significant because they contain index fluctuations of high frequency and amplitude. Although the research presented here primarily concerns cells, in understanding scattering from tissue, fibrous components such as collagen and elastin must be considered in addition to cellular matter. The relative importance of fibrous and cellular components depends on tissue type.

2. Methods

A. Yee's Method

Yee's method can be used to solve Maxwell's curl equations using the FDTD technique.¹² The algorithm takes Maxwell's curl equations and discretizes them in time and space, yielding six coupled finite-difference equations. The six electric and magnetic field components ($E_x, E_y, E_z, H_x, H_y, H_z$) are spatially and temporally offset on a three-dimensional grid. The grid spacing must be less than $\lambda/10$ to yield accurate results. Except when otherwise noted, a $\lambda/20$ grid was used for the simulations presented in this paper. As the six finite-difference equations are stepped in time, the electric and magnetic fields are updated for each grid point. To simulate propagation in an unbounded medium, boundary conditions must be applied to the tangential electric field components along the edges of the computational boundary at each time step. The Liao boundary condition is used in this paper.¹³ The incident wave is a sinusoidal plane-wave source.

The FDTD method computes the fields in a region around the cell that lies in the near field, which is then transformed to the far field. Parameters such as asymmetry parameter and scattering cross section can be computed from the scattering pattern. The details of the FDTD model used in this research and the relevant equations have been published previously and are not repeated here.¹⁰

B. Simulation Parameters

The cell is constructed by assigning permittivity values to each cell component. If desired, a range of permittivity values may be assigned to one component if that component, for example, the nucleus, is inhomogeneous. The equation for complex permittivity contains a frequency-dependent conductivity term.¹⁴ However, for a purely real refractive index, the dielectric constant at a particular wavelength is simply the square of the frequency-dependent refractive index.

To accurately determine scattering patterns, it is necessary to model the cells in as physically realistic a manner as possible. Information about the size, quantity, and dielectric structure of cellular organelles was obtained from the literature and by examining phase contrast images and electron micrographs of cell and organelles of interest. Re-

Table 1. Index of Refraction Values Obtained from the Literature

Organelle	Refractive Index	Reference
Extracellular fluid	1.35–1.36	18
Cytoplasm	1.36–1.375	15
Nucleus	1.38–1.41	15
Mitochondria and organelles	1.38–1.41	19
Melanin	1.6–1.7	20

fractive index is a function of the concentration of macromolecules in a particular organelle. However, an organelle's composition can vary significantly among different types of cells. For example, it has been reported that the refractive index of the nucleus is higher than that of the cytoplasm in Chinese hamster ovary cells¹⁵ and breast epithelial cells,¹⁶ whereas the cytoplasm was found to have a higher index than the nucleoid in *E. coli*.¹⁷ Thus accurate modeling of dielectric structure requires specific knowledge of organelle composition for the cell type of interest. Because this information is not readily available, refractive-index values from the literature were assembled as a starting point for the simulations. The nucleus was always modeled with some inhomogeneities in refractive index. The distribution of index variations employed in the simulations was based on Fourier analysis of 100× phase contrast images of normal and cancerous human breast epithelial cells. The general ranges of refractive index values used in the FDTD simulations are shown in Table 1.^{15,18–20}

C. Goniometer

A goniometer can be used to experimentally measure the phase function of an optically thin tissue section or dilute cell suspension. These measurements can then be compared with FDTD predictions or to other phase function approximations such as Mie theory or Henyey–Greenstein formulations. The goniometer setup is depicted in Fig. 1. An unpolarized 5-mW He–Ne laser ($\lambda = 612$ nm) is incident upon a cylindrical sample cell (1 cm). The cell is contained in a 31-cm tank filled with water for index-matching purposes. An incoherent fiber-optic bundle (1.5875 mm in diameter) is actuated about 160° beginning from the laser point of entry. A stepper motor under the control of a computer moves the fiber. The fiber is

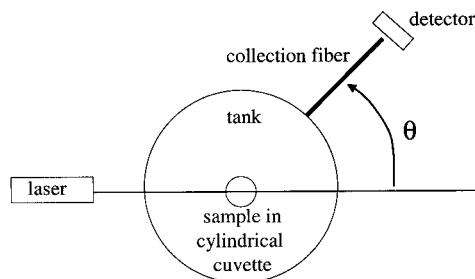


Fig. 1. Schematic diagram of a goniometer built to measure light scattering as a function of angle.

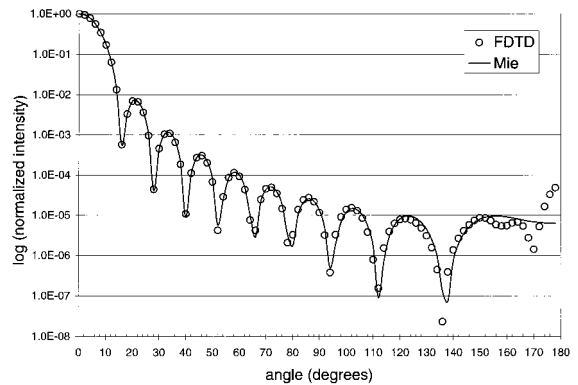


Fig. 2. Validation of the FDTD code. Comparison of FDTD results with Mie theory predictions for a 5- μ m sphere ($m = 1.04$; $\lambda = 900$ nm).

attached to the arm of the goniometer, which extends from the motor shaft and is designed to have an adjustable length (5–14 cm), permitting trade-offs between detected power and angular resolution. A prism with an aluminized hypotenuse for near 100% reflection is used to direct light into the fiber. An aperture on the prism face limits the effective N.A. of the fiber. The fiber delivers the light to a photodiode (Newport Model 835). Power is recorded to the computer using a general-purpose interface bus. A typical measurement with 2° angular resolution takes approximately 2 min.

3. Results: Simulations

A. Verification

The simulation program was verified by computing the scattering patterns of homogeneous spheres ranging in diameter from 0.5 to 10 μ m and comparing the results with Mie theory. For small spheres, the two curves agree closely for all angles at horizontal and vertical polarizations. For larger spheres, the FDTD pattern agrees well for most angles but is somewhat greater than the Mie pattern for angles higher than 160°. The artificial increase is due to imperfect boundary conditions, resulting in artificial reflections at the edges of the computational domain. The scattering pattern of a 5- μ m sphere is shown in Fig. 2. The asymmetry parameter g and scattering cross section differ from theoretical values by less than 0.2%, despite the artificial reflections.

In this paper we present the output of our model in two ways. We show scattering patterns, which we define to be a plot of the intensity of scattered light as a function of angle. When the scattered power is normalized to the value at 0°, we refer to the curve as a normalized scattering pattern. Alternatively, we present the scattering phase function, which presents the scattered power versus angle, where the area under the curve is normalized to one. In the scattering pattern, it is visually easier to assess the relative magnitude of scattered power at particular angles when comparing results from multiple simulations. However, when comparing FDTD data with

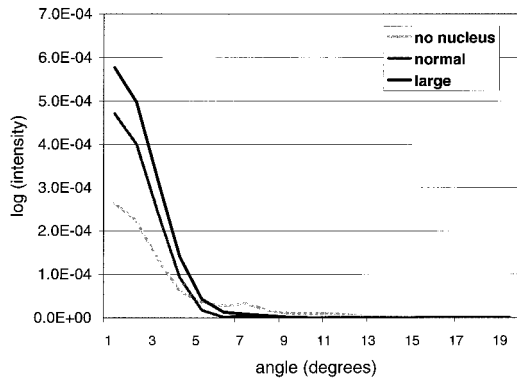


Fig. 3. Influence of nuclear structure on scattering pattern. Low-angle scatter is shown on a linear scale. There were no visible differences in scattering patterns at angles over 20° .

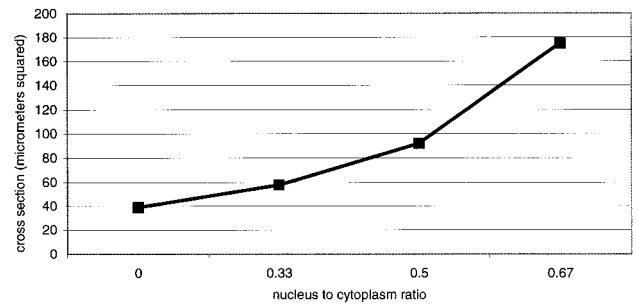
Mie theory or Henyey–Greenstein phase functions, data must first be normalized to an area of one. Methods for obtaining the phase function, asymmetry parameter, and scattering cross sections from raw data have been described previously.¹⁰

B. Influence of the Nucleus

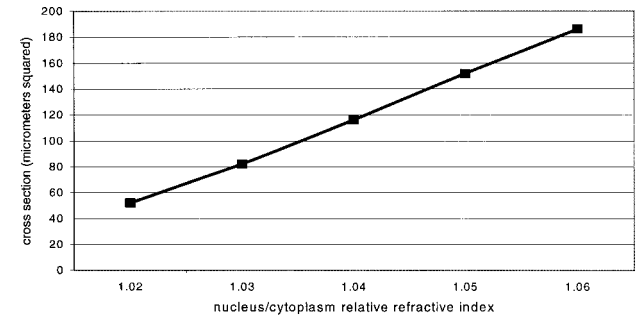
It is important to understand the effect of nuclear morphology on scattering properties because nuclear morphology is dramatically altered in cancerous cells. In general, cancerous cells have an increased nuclear-to-cytoplasmic (N/C) ratio.²¹ In addition, because cancerous cells divide more rapidly than normal cells and often have extra chromosomes, the protein concentration of the nucleus may be higher, altering nuclear refractive index. Also, there are changes in nuclear shape and texture as cells become cancerous.²¹

We used the FDTD model to study the relationship between the physical structure of the nucleus and its scattering properties, examining separately the effects of nuclear size and nuclear refractive index on the scattering pattern. Unless otherwise specified, all simulations presented in this paper involved a $15\text{-}\mu\text{m}$ -diameter spherical cell containing cytoplasm, a nucleus, and organelles of multiple sizes and shapes. Wavelength of incident light was 900 nm . To isolate changes that are due to the nucleus, the volume fraction of other organelles was kept low (0.02%), and a small mismatch between cytoplasm and extracellular fluid ($m = 1.014$) was employed. Note that we define m to be a relative index of refraction (in this case, between cytoplasm and extracellular fluid) and n to be an absolute index of refraction. Nuclear index variations were uniformly distributed between $\Delta n = \pm 0.03$ about the mean nuclear index, $n = 1.39$, at spatial frequencies ranging from 2 to $20\ \mu\text{m}^{-1}$.

Scattering patterns were calculated for cells with nuclei of diameter 0 , 5 , 7.5 , and $10\ \mu\text{m}$. Increases in nuclear size create noticeable changes in the scattering pattern at small angles. Figure 3 shows the small-angle scattering patterns of a $15\text{-}\mu\text{m}$ cell with



(a)



(b)

Fig. 4. (a) Influence of N/C ratio on scattering cross section. (b) Influence of relative N/C refractive index on scattering cross section.

no nucleus, a small nucleus ($5\ \mu\text{m}$ in diameter), and a large nucleus ($10\ \mu\text{m}$ in diameter). The higher-angle (over 20°) scattering of cells containing nuclei of various sizes is highly dependent on factors such as incident wavelength and refractive-index structure of the nuclei. For example, when cells are modeled with homogeneous nuclei, high-angle scattering is not significantly altered as nuclear size is increased.²² However, when the nucleus is modeled as a heterogeneous structure, high-angle scattering increases with increasing nuclear size.²²

Scattering cross section significantly increases as the N/C ratio rises [Fig. 4(a)]. In this paper we define the N/C ratio as the diameter of the nucleus divided by the diameter of the cytoplasm. Scattering cross section also increases as the relative N/C refractive index is increased [Fig. 4(b)]. For nuclear sizes and index of refraction values within the range expected for biological cells, there appears to be a linear relationship between relative N/C refractive index and scattering cross section; the relationship between the N/C ratio and the scattering cross section is of higher order.

C. Influence of Organelles

To investigate the effect of small cytoplasmic organelles, three simulations were conducted. For each of the three cases, a $15\text{-}\mu\text{m}$ spherical cell with a $5\text{-}\mu\text{m}$ nucleus (mean $m = 1.02$; spatial fluctuations between 2 and $20\ \mu\text{m}^{-1}$) was created. In addition to the nucleus, the first cell contained an 8.5% volume fraction of melanin ($n = 1.65$; $1\text{-}\mu\text{m}$ sphere). Mela-

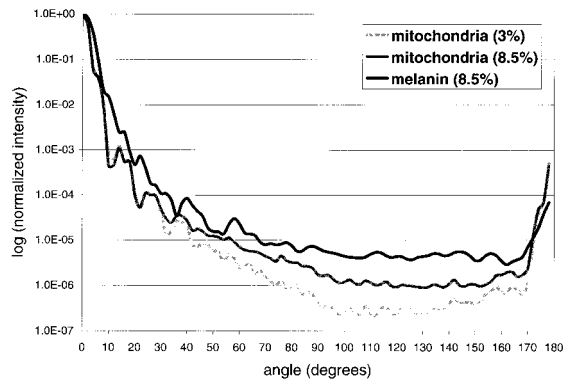


Fig. 5. Influence of internal structure on scattering pattern. Three simulations are shown: a cell containing organelles of refractive index and size consistent with melanin (8.5% volume fraction), a cell containing organelles with index and size of mitochondria (8.5% volume fraction), and an amelanotic cell containing organelles with index and size of mitochondria but a smaller volume fraction (3%).

nin was modeled with and without absorption. There was little difference in obtained results when absorption was incorporated as an imaginary component of the refractive index. Despite its high absorption coefficient, melanin causes little attenuation within a cell because path lengths are small. To compare the effects of melanin with an organelle of lower refractive index, a second cell was modeled containing an 8.5% volume fraction of organelles similar in size, shape, and refractive index to mitochondria (ellipsoids $\sim 0.5 \mu\text{m} \times 0.5 \mu\text{m} \times 1.5 \mu\text{m}$; $n = 1.41$). A third cell (amelanotic) was constructed similarly to the second cell but contained only a 3% organelle volume fraction. The scattering patterns from these simulations are shown in Fig. 5.

Figure 5 demonstrates that internal structure can have a strong influence on scattering pattern, particularly for angles over 40° . In the cells containing melanin and mitochondria, the total volume of organelles in the cell is identical. The difference in the two curves is due to the higher index of melanin relative to mitochondria. The melanin results in a scattering pattern that covers a smaller magnitude range than the other two curves. We define the magnitude range of a scattering pattern as the scattering pattern's maximum intensity value divided by the minimum intensity ($I_{\text{max}}/I_{\text{min}}$) value. Scattering cross section was also larger for a cell containing melanin rather than lower-index organelles. Scattering cross sections of cells containing melanin and mitochondria (8.5% volume fraction) and the amelanotic cell (3% volume fraction) were 861, 729, and 639 μm^2 , respectively. In general, increasing organelle volume fraction increases scattering cross section and makes the scattering pattern more isotropic.

D. Influence of Morphology

We investigated the influence of morphology on scattering patterns. For example, does it matter whether a cell is constructed by placing a certain

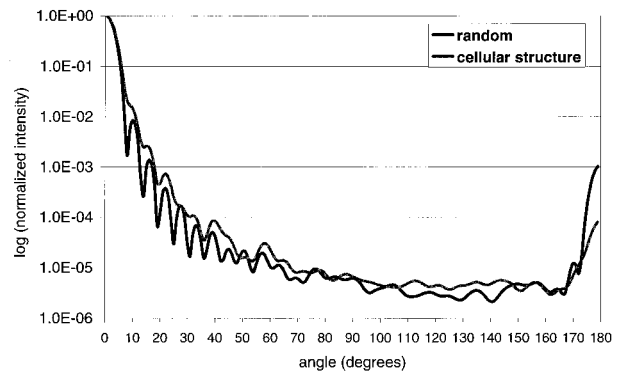


Fig. 6. Comparison of scattering pattern from a cell with a specified internal structure (cytoplasm, nucleus, and organelles) with a cell with randomly assigned dielectric structure. Mean index of both cells is identical, $n = 1.4$.

number of organelles of specific size and refractive index at explicit locations rather than randomly generating a dielectric structure, using a range of refractive indices and a chosen frequency of index fluctuations? To examine the difference between these two cases, the scattering pattern of a cell generated with specific morphology was compared with the scattering pattern of a cell constructed using random refractive-index assignments. To generate the cell without morphological structure, all grid points within the sphere were assigned refractive-index values, based on the desired frequency of spatial fluctuations in refractive index ($2\text{--}20 \mu\text{m}^{-1}$) and a chosen range of refractive-index values, uniformly distributed about a mean index ($n = 1.40 \pm 0.05$). The cell with known morphology is similar to the melanotic cell described in Subsection 3.C. Results are shown in Fig. 6. The overall shape and range of the scattering pattern is similar for a cell with random dielectric structure and a cell with specific morphology.

Figure 7 demonstrates the effect of changing the frequency of spatial variations while keeping the mean refractive-index value constant for a cell with

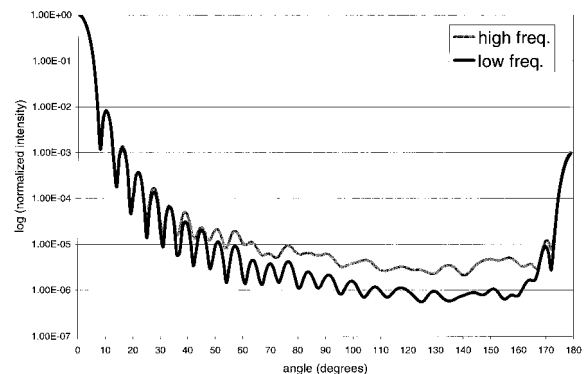


Fig. 7. Scattering pattern of two cells with randomly assigned dielectric structure. The spatial frequency of index fluctuations is higher in the top curve (labeled high frequency) than in the lower curve (labeled low frequency). Mean refractive index is the same for both cells.

randomly generated dielectric structure. The normalized scattering pattern for two cells are plotted. Both cells have a mean index of $n = 1.4$, with uniformly distributed variations between $n = 1.35$ and $n = 1.45$. In one cell the spatial frequency of the index variations ranges from 5 to $20 \mu\text{m}^{-1}$; in the other cell the spatial frequency of the variations ranges from 2 to $10 \mu\text{m}^{-1}$. The curves demonstrate that, as the frequency of refractive-index fluctuations is increased, the scattered intensity becomes higher at large angles.

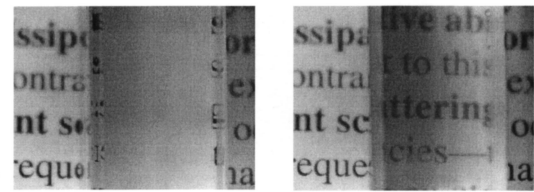
E. Influence of Extracellular Medium

Typically, in published simulations of cell scattering or goniometric measurements, the cell is surrounded by a low-index medium such as extracellular fluid ($n = 1.35$), blood ($n = 1.345$), growth medium ($n = 1.34$), or phosphate-buffered saline ($n = 1.33$).^{8,9,15,16,23} However, in tissue, cells are likely surrounded by other cells or tissue structures of higher index of refraction. When an object is bordered by other objects of similar index, rather than a medium of significantly lower index, scattering will be reduced because of index matching. To demonstrate this concept, we repeat an experiment first performed by Barer in the 1950's.²⁴ Figure 8(a) shows two images of cuvettes filled with an equal concentration of breast cancer cells ($10^6/\text{ml}$). In the cuvette on the left, the cells are immersed in saline solution ($n = 1.33$). Because of scattering from the cells, it is not possible to read the text behind the cuvette. In the cuvette on the right, the cells are immersed in an albumin solution ($n = 1.37$). Scattering is reduced and the text is readable.

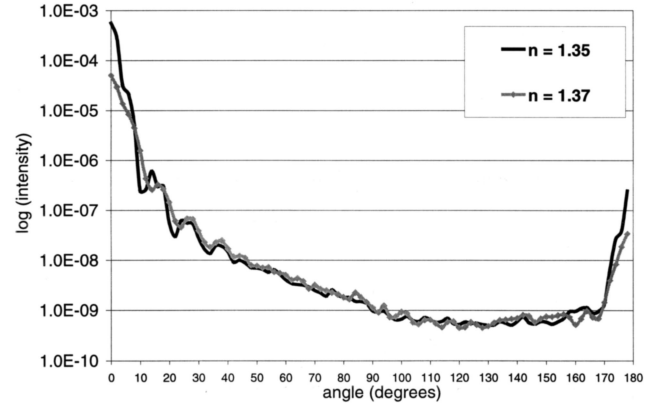
The FDTD model predicts the index-matching effect. Figure 8(b) shows the scattering pattern of an ovarian cancer cell immersed in solutions of different index of refraction: $n = 1.35$ and $n = 1.37$. When the index of the medium surrounding the cytoplasm is increased to more closely match the cytoplasm ($n = 1.37$), scattering at the lowest angles is reduced by almost an order of magnitude relative to the $n = 1.35$ case. Scattering cross section is reduced from 729 to $192 \mu\text{m}^2$ simply by decreasing the index mismatch by $\Delta n = 0.02$.

F. Scattering from a Collagen Fiber

To investigate the scattering pattern of collagen, a collagen fiber was modeled using a cylindrical geometry ($3 \mu\text{m}$ in diameter, $20 \mu\text{m}$ in length). The collagen fiber was composed of a number of fibrils oriented along the long axis of the cylinder. The diameter of the fibrils ranged from 60 to 240 nm. The fibrils contained cross striations approximately every 60 nm in length. These cross striations were implemented through refractive-index fluctuations. The refractive index of collagen has been measured to be between $n = 1.46$ and 1.55 .²⁵ The high end of this range was measured using dried collagen and is not realistic for *in vivo* tissues. The simulation reported here used a mean value for collagen of $n = 1.46$ ($\Delta n = \pm 0.04$). The extracellular matrix surrounding collagen can vary from watery to a gellike consistency,



(a)



(b)

Fig. 8. (a) As a visible demonstration of reduction in scattering that is achievable by immersing cells in a solution of like index, two cuvettes are shown with equal concentrations of cells. In the cuvette on the left, cells are immersed in saline ($n = 1.33$); in the cuvette on the right, cells are immersed in a higher-index albumin solution ($n = 1.37$). Index matching reduces the scattering, and the text behind the cuvette is readable. (b) Influence of external medium on scattering pattern. The scattering patterns of the same cell immersed in media of varying index ($n = 1.35$, $n = 1.37$) are compared.

altering its refractive index. For this experiment, the index of refraction of the extracellular matrix was set at $n = 1.36$.

The calculated scattering pattern of a collagen fiber is shown in Fig. 9. The scattering patterns shown are the patterns for three different orientations of the

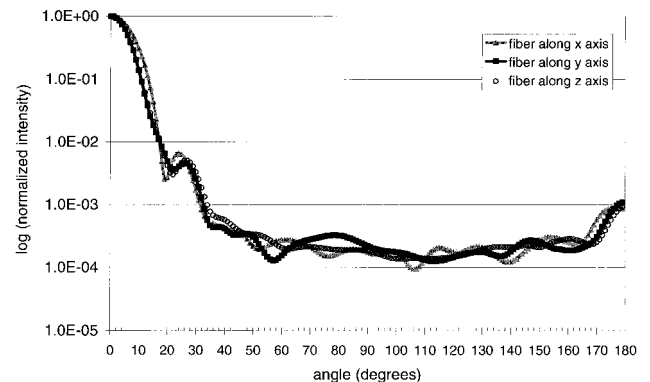


Fig. 9. Scattering pattern of a collagen fiber. Curves shown are for three orientations of the collagen fiber with respect to an incoming plane wave along the $+z$ axis. The collagen fibers were oriented along the x , y , and z axes, respectively.

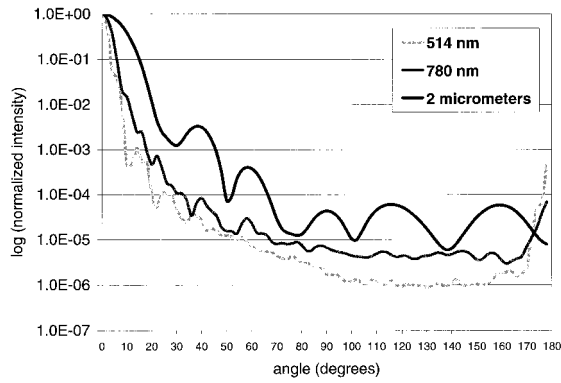


Fig. 10. Wavelength dependence of scattering pattern. The normalized scattering pattern of one cell is shown for three wavelengths (514 nm, 780 nm, 2 μm).

collagen fiber with respect to an incoming plane wave in the $+z$ direction. The collagen fiber was placed along the x , y , and z axes for the three trials. As is the case for cells, the scattering pattern is highly peaked in the forward direction. The number of orders of magnitude covered by the scattering pattern ($I_{\text{max}}/I_{\text{min}}$) is lower for collagen than a cell by 1 to 2 orders of magnitude.

G. Wavelength Dependence of Scattering Pattern

To investigate the wavelength dependence of cellular scattering, scattering from the same cell was simulated for wavelengths of 514 nm, 780 nm, and 2 μm . The results are shown in Fig. 10. As evidenced by Fig. 10, changes in wavelength, even in the visible portion of the spectrum, produce significant changes in the scattering. As the wavelength increases with respect to the size of the scatterers, the number of peaks in the curves decrease. This can be predicted qualitatively from a decrease in the average Mie size parameter. It should be noted that little experimental data are available concerning the dispersion of cell constituents other than water. The simulations shown here illustrate only the influence of changes in incident wavelength relative to the size of the scattering particles, not the influence of dispersion. However, over the range of wavelengths simulated here, the relative indices of refraction do not change significantly.

We also investigated the wavelength dependence of scattering cross section. Recently, Perelman *et al.*²⁶ presented a technique for extracting nuclear size distributions from measurements of tissue backscattering. A fundamental assumption of the technique is that the optical scattering cross section, $\sigma_s(\lambda, l)$, of the nucleus of a cell can be predicted using the van de Hulst (anomalous diffraction) approximation²⁷:

$$\sigma_s(\lambda, l) = \frac{1}{2} \pi l^2 \left\{ 1 - \frac{\sin(2\delta/\lambda)}{\delta/\lambda} + \left[\frac{\sin(\delta/\lambda)}{\delta/\lambda} \right]^2 \right\}, \quad (1)$$

where $\delta = \pi n_c l(m - 1)$. In Eq. (1), n_c is the refractive index of cytoplasm, m is the refractive index of the nucleus relative to that of cytoplasm, and l is the

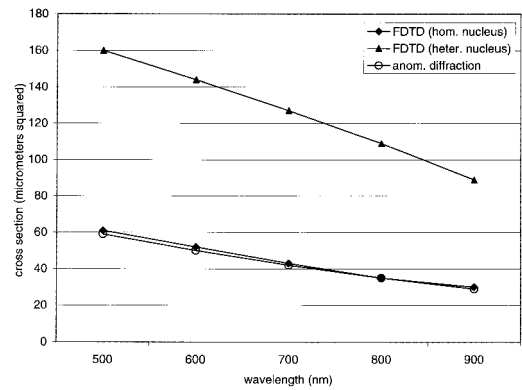


Fig. 11. Scattering cross section versus wavelength for nucleus surrounded by cytoplasm. Three cases are shown. First, the van de Hulst approximation (anomalous diffraction approximation) is used to calculate scattering for a 5- μm nucleus ($m = 1.04$; $n_{\text{cytoplasm}} = 1.36$). Second, the FDTD model is used to calculate scattering for a homogeneous 5- μm nucleus ($m = 1.04$; $n_{\text{cytoplasm}} = 1.36$). Third, the FDTD model is used to calculate scattering for a heterogeneous 5- μm nucleus, with mean relative refractive index identical to the homogeneous case and spatial fluctuations ranging from 2 to 30 μm^{-1} .

diameter of the nucleus. The van de Hulst approximation assumes that the nucleus of a cell can be modeled as a homogeneous sphere.

We compared FDTD predictions for optical scattering cross section for inhomogeneous nuclei with results obtained using the van de Hulst approximation for wavelengths between 500 and 900 nm. The van de Hulst approximation was computed for a 5- μm -diameter nucleus, $n = 1.04$, surrounded by cytoplasm, $n_c = 1.36$. Two sets of FDTD computations were considered. First, the nucleus was modeled as a 5- μm sphere, $m = 1.04$, surrounded by cytoplasm, $n_c = 1.36$. This produces the same results that would be predicted by Mie theory. The comparison of FDTD homogeneous sphere results with results from the van de Hulst approximation (Fig. 11) demonstrates that the van de Hulst approximation is valid in this wavelength and particle diameter region. For the second set of FDTD simulations, the nucleus was modeled as an inhomogeneous sphere surrounded by cytoplasm, with nuclear index uniformly distributed between $m = 1.01$ and $m = 1.07$ (mean $m = 1.04$). The frequency of spatial variations ranged from 2 to 30 μm^{-1} . A 33-nm grid spacing was used for all wavelengths so that the same spatial frequency fluctuations could be simulated for all cases. As shown in Figure 11, FDTD results for an inhomogeneous cell predict a similar cross section versus wavelength trend to that predicted by the van de Hulst approximations. However, the cross-sectional values predicted for an inhomogeneous nucleus are a factor of 2–3 higher.

4. Results: Experiments

A. Validation

To compare theoretical predictions of light scattering to physical measurements, a goniometer was con-

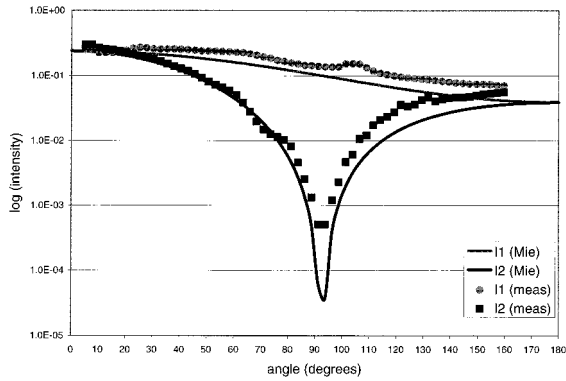


Fig. 12. Validation of goniometer performance. Comparison of measured data and Mie theory predictions for 0.2- μm polystyrene spheres.

structured. To demonstrate that the goniometer was functioning properly, measurements were made on dilute suspensions of 0.2- μm polystyrene spheres (Bangs Laboratories). A linear polarizer was introduced to allow measurement of horizontal and vertical polarizations. The two polarizations result in different scattering patterns for 0.2- μm spheres. The measured scattering patterns are plotted in Fig. 12 along with the corresponding curves from Mie theory. Commercially available software (MIETAB) was used for the Mie theory calculation. The measured scattering patterns agree well with the theoretical curves. The increased measured values relative to Mie theory predictions near 90° are due to the finite angular resolution of the goniometer rather than a limitation in dynamic range of the detector which is 5–6 orders of magnitude.

B. Cell Measurements

The scattering pattern of a suspension of cultured ovarian cancer cells (OVCA-420 cells) was measured using the goniometer. The cells were measured suspended in isotonic phosphate-buffered saline ($n = 1.33$) at concentrations of approximately 10^5 cells/ml. This concentration was determined by repeated dilution of a concentrated solution of 10^6 cells/ml. After each dilution, the scattering pattern of the cells was measured in the goniometer. Measurements were repeated with progressively more-dilute solutions until further dilution did not influence the results in the manner described by Mourant *et al.*²³ The total transmission of the final dilution was ~ 0.94 at $\lambda = 612$ nm. The diameter of the cells was approximately 10 μm with a 6- μm nucleus.

The measured phase function for a dilute suspension of OVCA cells is plotted in Fig. 13. Values below 6° are obtained by linear extrapolation of logarithmic intensity data. Figure 13 also shows a comparison of measured results with those predicted by the FDTD model (averaged over three orientations of the cell with respect to the incident light) for an OVCA cell measured and simulated at $\lambda = 612$ nm. Modeled cell parameters were based on phase contrast observations of OVCA cells. The modeled cell

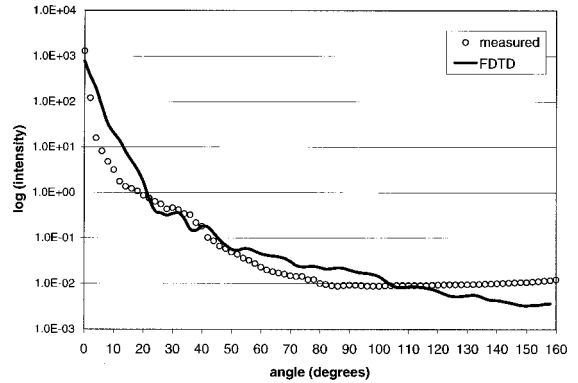


Fig. 13. Comparison of measured and FDTD data for OVCA-420 cells. The FDTD data are the average over two orientations of the cell with respect to incident light.

was a 10- μm cell with a 6- μm -diameter nucleus. The nucleus contained spatial variations in the refractive index at a spatial frequency of approximately $2 \mu\text{m}^{-1}$ with $\Delta n = \pm 0.03$. Data concerning the volume fraction of organelles in OVCA cells were not available; a volume fraction of 10% was used in the simulation. The results show that, with some knowledge about a cell's structure and by averaging FDTD results for the same cell at a few orientations relative to incident light, it is possible to reasonably model the physically measurable scattering pattern. The accuracy could be improved by increased knowledge of cellular contents and dielectric structure.

Figure 14 shows the measured data compared with Henyey–Greenstein and Mie theory predictions. The Henyey–Greenstein phase function used an asymmetry value of $g = 0.97$, computed from the measured scattering pattern. The Mie phase function was calculated using unpolarized light ($\lambda = 612$ nm) for a 10- μm sphere, $n = 1.38$, surrounded by phosphate-buffered saline, $n = 1.33$. For this cell, the Henyey–Greenstein phase function underestimated high-angle scatter. The Mie phase function was a poor fit, underestimating high-angle scatter by up to 2 orders of magnitude.

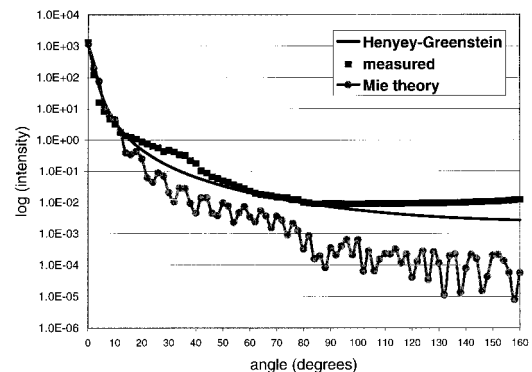


Fig. 14. Comparison of measured scattering pattern with Mie theory (10- μm sphere, $m = 1.04$, $\lambda = 612$ nm) and Henyey–Greenstein predictions. Asymmetry value of $g = 0.97$, calculated from measured data, was used in the Henyey–Greenstein model.

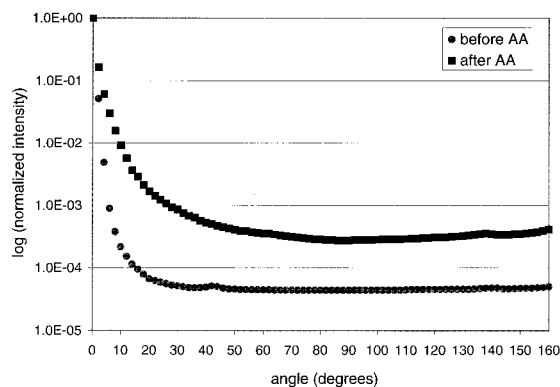


Fig. 15. Measurements of a cervical cancer cell line before and after addition of 6% acetic acid (AA).

C. Influence of Acetic Acid

Acetic acid is used during colposcopy to enhance differences in the diffuse reflectance of normal and diseased regions of the cervical epithelium.²⁸ Transient whitening of tissue after the application of acetic acid serves as a simple and inexpensive method for identification of areas that may eventually develop into cervical cancer. To explore the effect of acetic acid on cell scattering, cervical cancer cells (He-La cell line) were exposed to 6% acetic acid. The scattering pattern of the cells was measured immediately before and after exposure to acetic acid. The measured scattering of He-La cells before and after exposure to acetic acid is shown in Fig. 15. Increased scattering is apparent at most angles.

As another test of the influence of acetic acid, FDTD simulations were conducted on a cell before and after the addition of acetic acid. Changes to the simulated cell were based on phase contrast and confocal microscope images of cells before and after acetic acid.²⁹ These images indicate that the predominant effect of acetic acid is an alteration of the refractive-index structure of the nucleus. In the FDTD simulation of a cell before and after addition of acetic acid, nuclear index fluctuations were of increased frequency (before addition, $2\text{--}10\ \mu\text{m}^{-1}$; after addition, $2\text{--}20\ \mu\text{m}^{-1}$) and higher magnitude (before addition, $\Delta n = \pm 0.03$; after addition, $\Delta n = \pm 0.06$) after the introduction of acetic acid. A cross section for the cell after addition of acetic acid increased from 519 to $843\ \mu\text{m}^2$.

5. Discussion

An obvious question about a model as computationally intensive as the FDTD method is whether such an approach is really necessary. Are simple analytical descriptions such as those provided through Mie theory or Henyey–Greenstein approximations sufficient? It is our belief that simple analytical descriptions of cellular scattering are only adequate for some purposes. For example, if a Monte Carlo model is used to calculate total tissue reflectance or transmittance, approximations such as Henyey–Greenstein or Mie theory are likely to produce acceptable results. However, if the same Monte Carlo model is used to

simulate a typical endoscopic situation, in which the light delivery and collection fibers are near to each other, the choice of phase function will significantly affect the number of photons collected. The influence of phase function on light transport for small source detector separations has been demonstrated previously by Mourant *et al.*³⁰ The results of Mourant's simulations demonstrate the necessity of choosing a phase function that accurately reflects the probability of high-angle scatter when small source detector separations are used.

We believe a more flexible and realistic approach such as that provided by the FDTD solution is the only way to estimate the accuracy of current Mie theory and Henyey–Greenstein approximations. In addition, we believe that there is valuable information about the interaction of light with a single cell that can be obtained from our more complicated approach. For example, we find that the overall shape of the nucleus influences small-angle scattering whereas the effects of small intracellular organelles, or high-frequency index of refraction fluctuations, are more evident at higher angles. We believe that understanding these types of trends not only develops fundamental knowledge of the interaction of light with a single cell, but also serves a practical purpose in facilitating the design of more effective optical diagnostic systems by allowing prediction of changes in scattering as a function of cell morphology.

Currently, limitations in the knowledge of cellular composition and dielectric structure make it difficult to construct a specific type of cell, simulate it, and conclude that the obtained scattering pattern is exactly what would be obtained through experimental measurements of the scattering from that kind of cell. However, the simulations presented in this paper clearly establish that scattering patterns change significantly based on the cell's internal structure, the surrounding environment, and the wavelength of illuminating light. Thus using one phase function such as the Henyey–Greenstein phase function or a Mie theory approximation to represent a typical cell is probably unrealistic. Henyey–Greenstein phase functions have been shown to poorly describe high-angle scattering. This was documented recently by Mourant *et al.*²³ and is further supported by the experimental measurements presented in this research. Mie theory approximations are severely limited because they do not account for internal structures, which are expected to be the primary source of cellular scattering in *in vivo* measurements.

The FDTD simulations document the influence of organelle volume fraction and refractive index on cellular scattering. Both volume fraction and refractive index of cell components will be highly variable in biological cells and will depend on cell type. Although it is possible to qualitatively predict trends in phase function or scattering cross section as the refractive index and volume fraction are varied, the FDTD method provides more quantitative information. The simulations suggest that it is possible to consider increasing the size and spatial variations of

the nucleus as analogous to changing organelle volume fraction. The similarity of cells simulated with specific morphology to those with randomly generated dielectric structure suggests that it is the overall frequency and magnitude of index of refraction fluctuations, rather than a particular spatial arrangement of cell components, which has the more crucial effect on a cell's scattering pattern. The effect of high-frequency fluctuations, which can be viewed as small scatterers, is particularly apparent at high angles. In a cell, high-frequency fluctuations in refractive index might be created by components such as microtubules, membranes, chromatin, or other organelle constituents.

The FDTD method can also provide information about the relative importance of scattering from cellular matter and extracellular fibrous proteins in tissue. Comparing the scattering pattern of collagen with that of a cell, it is evident that the likelihood of high-angle scattering events is markedly increased for fibrous tissue components such as collagen. For optical techniques sensitive to high-angle scatter, it is possible that collagen could dominate scattering from cells when the volume of interrogation includes a layer of cells lying on top of a layer of collagen. Potentially, scattering from collagen could prove problematic in the detection of dysplasia in epithelial tissues. Dysplastic changes originate near the basal layer and propagate upward. Scattering from the reticular fibers in the basal layer and underlying stroma might override more subtle scattering changes caused by nuclear abnormalities and mitotic activity in mildly dysplastic cells. This suggests that weakly confocal probes that restrict the volume of interrogation to the epithelium might be useful to avoid measuring scattering from collagen when examining epithelial tissues.

The simulations and measurements presented here illustrate the profound differences that the index of the surrounding medium can have on the cell scattering pattern. Thus it is important to recognize the difference between measuring and simulating cells in suspensions compared with those in real tissue. A large portion of the measured or predicted scattering for cells suspended in saline occurs because of the mismatch in refractive index between the cells and its surrounding, a mismatch that may not be realistic for *in vivo* tissue. Goniometric measurements on cells should be performed in a medium of higher index to measure scattering that is due to internal structure, rather than scattering from the cell and phosphate-buffered saline border. Practically, this is not easily accomplished because the immersion medium must be a substance that does not alter or harm the cell. Albumin, a useful protein for index matching in phase contrast microscopy experiments, scatters too significantly to be used to increase the refractive index of the immersion medium in goniometry. Proteins smaller than albumin may offer a potential alternative.

The measurements of scattering from cell suspensions reported here are similar to the measurements

of fibroblast suspensions by Mourant *et al.*²³ In both cases, the data presented do not show the interference peaks found in Mie theory predictions. A biological cell contains scatterers with a wide range of sizes. This wide range of scatterer sizes may eliminate the peaks that are present in Mie theory predictions that assume scatterers of only one size. Schmitt and Kumar have shown previously that when a distribution of scatterer sizes is assumed rather than a single size, the phase functions become smoother curves with fewer peaks, which is much more similar to what we measure.⁵ Another factor that may contribute to the smoothness of measured phase functions is the random orientation of cells in suspension.

Finally, the simulations and measurements presented here illustrate the potential importance of acetic acid as a contrast agent in optical diagnostics. Whether considering FDTD predictions, goniometric measurements, or the images from both phase contrast and confocal microscopy recently presented by Smithpeter *et al.*,²⁹ acetic acid has been shown to increase scattering from a cell. It has been suggested in the literature that the acetowhitening effect seen in cervical tissue is due to coagulation of nuclear proteins.²⁸ Based on our own phase contrast microscopy observations of the effects of acetic acid,²⁹ we suspect that acetic acid changes the size of scatterers in the nucleus, resulting in an increase in the magnitude and frequency of fluctuations in refractive index. Although the importance of acetic acid in accurate colposcopic diagnosis has been recognized for many years, we believe that acetic acid may also prove extremely significant in quantitative optical diagnosis of precancerous conditions because of acetic acid's ability to selectively enhance nuclear scatter.

6. Conclusions

We have presented the application of the FDTD technique for examination of light-scattering properties of biological cells and tissue structures. Although computationally intensive, the method places no limitations on the geometry or index structure of the objects under question. The model can be used to study the effect of changes of wavelength and of cellular biochemical and morphological structure. The data obtained from the model can be used to calculate phase functions, scattering cross section, and asymmetry parameter. As the data demonstrate, relatively small changes in internal structure, external medium, and wavelength can significantly change both phase function and scattering cross section. This suggests that phase functions that are more flexible than Mie theory or Henyey-Greenstein may be useful to improve the accuracy of optical modeling techniques. Currently, the utility of the FDTD technique is limited by lack of adequate knowledge concerning cellular dielectric structure. As this knowledge is developed, the FDTD method will become increasingly valuable.

The authors thank the High Performance Computing Facility at the University of Texas at Austin for a computer time grant on a Cray J90 supercomputer. The authors also express their appreciation to Kimberly Kline, Marla Simmons-Mechaca, Robert Bast, and Dafna Lotan for assistance in obtaining and preparing cell samples.

References

1. M. Rajadhyaksha, M. Grossman, D. Esterwitz, R. Webb, and R. Anderson, "In-vivo confocal scanning laser microscopy of human skin: melanin provides strong contrast," *J. Invest. Dermatol.* **104**, 946–952 (1995).
2. J. Izaat, M. Hee, D. Huang, A. Swanson, C. Lin, J. Schuman, C. Puliafito, and J. Fujimoto, "Micron-resolution biomedical engineering with optical coherence tomography," *Opt. Photon. News* **4**, 14–19 (1993).
3. J. Mourant, I. Bigio, J. Boyer, R. Conn, T. Johnson, and T. Shimada, "Spectroscopic diagnosis of bladder cancer with elastic light scattering," *Lasers Surg. Med.* **17**, 350–357 (1995).
4. J. Fishkin, O. Coquoz, E. Anderson, M. Brenner, and B. Tromberg. "Frequency-domain photon migration measurements of normal and malignant tissue optical properties in a human subject," *Appl. Opt.* **36**, 10–20 (1997).
5. J. Schmitt and G. Kumar, "Optical scattering properties of soft tissue: a discrete particle model," *Appl. Opt.* **37**, 2788–2797 (1998).
6. A. Brunsting and P. Mullaney, "Light scattering from coated spheres: model for biological cells," *Appl. Opt.* **11**, 675–680 (1972).
7. G. Streekstra, A. Hoekstra, E. Nijhof, and R. Heethaar, "Light scattering by red blood cells in ektacytometry: Fraunhofer versus anomalous diffraction," *Appl. Opt.* **32**, 2266–2272 (1993).
8. G. Videen and D. Ngo, "Light scattering multiple solution for a cell," *J. Biomed. Opt.* **3**, 212–220 (1998).
9. A. Nilsson, P. Alsholm, A. Karlsson, and S. Andresson-Engels, "T-matrix computations of light scattering by red blood cells," *Appl. Opt.* **37**, 2735–2748 (1998).
10. A. Dunn and R. Richards-Kortum, "Three-dimensional computation of light scattering from cells," *IEEE J. Sel. Top. Quantum Electron.* **2**, 898–905 (1996).
11. B. Beauvoit, T. Kitai, and B. Chance, "Time-resolved spectroscopy of mitochondria, cells, and rat tissue under normal and pathological conditions," in *Photon Transport in Highly Scattering Tissue*, S. Avrillier, B. Chance, G. J. Mueller, A. V. Priezzhev, and V. V. Tuchin, eds., *Proc. SPIE* **2326**, 127–136 (1995).
12. L. Junqueira, J. Carneiro, and O. Kelly, *Basic Histology* (Appleton and Lange, New York, 1992).
13. Z. Liao, H. Wong, B. Yang, and Y. Yuan, "A transmitting boundary for transient wave analysis," *Sci. Sin. Ser A* **27**, 1063–1076 (1984).
14. E. Hecht, *Optics* (Addison-Wesley, Reading, Mass., 1987).
15. A. Brunsting and P. Mullaney, "Differential light scattering from spherical mammalian cells," *Biophys. J.* **14**, 439–453 (1974).
16. R. Drezek, "Finite difference time domain simulations and goniometric measurements of light scattering from cells," M.S. thesis (University of Texas at Austin, Austin, Texas, 1998).
17. J. Valkenburg and C. Woldringh, "Phase separation between nucleoid and cytoplasm in *E. coli* as defined by immersive refractometry," *J. Bacteriol.* **160**, 1151–1157 (1984).
18. J. Maier, S. Walker, S. Fantini, S. Franceschini, and E. Gratton, "Possible correlation between blood glucose concentration and the reduced scattering coefficient of tissues in the near infrared," *Opt. Lett.* **19**, 2062–2064 (1994).
19. H. Liu, B. Beauvoit, M. Kimura, and B. Chance, "Dependence of tissue optical properties on solute-induced changes in refractive index and osmolarity," *J. Biomed. Opt.* **1**, 200–211 (1996).
20. I. Vitkin, J. Woolsey, B. Wilson, and R. Anderson, "Optical and thermal characterization of natural (sepia officinalis) melanin," *Photochem. Photobiol.* **59**, 455–462 (1994).
21. C. Boone, G. Kelloff, and V. Steele, "The natural history of intraepithelial neoplasia: relevance to the search for intermediate endpoint biomarkers," *J. Cell. Biochem.* **16**, 23–26 (1992).
22. A. Dunn, "Light scattering properties of cells," Ph.D. dissertation (University of Texas at Austin, Austin, Texas, 1997).
23. J. Mourant, J. Freyer, A. Hielscher, A. Eick, D. Shen, and T. Johnson, "Mechanisms of light scattering from biological cells relevant to noninvasive optical-tissue diagnostics," *Appl. Opt.* **37**, 3586–3593 (1998).
24. R. Barer, "Refractometry and interferometry of living cells," *J. Opt. Soc. Am.* **47**, 545–556 (1957).
25. Y. Yarker, R. Aspden, and D. Hukins, "Birefringence of articular cartilage and the distribution of collagen fibril orientations," *Connect. Tissue Res.* **11**, 207–213 (1983).
26. L. Perelman, V. Backman, M. Wallace, G. Zonios, R. Manoharan, A. Nustrat, S. Shields, M. Seiler, C. Lima, T. Hamano, I. Itzkan, J. Van Dam, J. Crawford, and M. Feld, "Observation of periodic fine structure in reflectance from biological tissue: a new technique for measuring nuclear size distribution," *Phys. Rev. Lett.* **80**, 627–630 (1998).
27. H. C. van de Hulst, *Light Scattering by Small Particles* (Dover, New York, 1957).
28. M. Anderson, J. Jordon, A. Morse, and F. Sharp, *A Text and Atlas of Integrated Colposcopy* (Mosby, St. Louis, Mo., 1993).
29. C. Smithpeter, A. Dunn, R. Drezek, T. Collier, and R. Richards-Kortum, "Near real time confocal microscopy of cultured amelanotic cells: sources of signal, contrast agents, and limits of contrast," *J. Biomed. Opt.* **3**, 429–436 (1998).
30. J. Mourant, J. Boyer, A. Hielscher, and I. Bigio, "Influence of the scattering phase function on light transport measurements in turbid media performed with small source-detector separations," *Opt. Lett.* **21**, 546–548 (1996).